 doi:10.20944/preprints202205.0389.v1

Article

Performance Evaluation of Roughened Solar Air Heaters for Stretched Parameters

Mustafa Alaskari [1], Arwa M. Kadhim [1], Ammar A. Farhan [1], Moustafa Al-Damouk [2], Mansour Al Qubeissi3

[1] Department of Energy Engineering, University of Baghdad, 10071, Baghdad, Iraq; mustafa.alaskari@coeng.uobaghdad.edu.iq (M.A), arwa.kadhem1009@coeng.uobaghdad.edu.iq (A.M.K), ammarali@uobaghdad.edu.iq (A.A.F)
[2] Renewable Energy Research Center, University of Anbar, Iraq; mustafa.adil@uoanbar.edu.iq
[3] Faculty of Engineering, Environment and Computing, Coventry University, Coventry CV1 2JH, United Kingdom; ac1028@coventry.ac.uk

Abstract: Artificial roughness applied to the Solar Air Heater (SAH)'s absorber plate is a popular technique to increase its total-thermal efficiency (η_{t-th}). In this paper, the influence of geometrical parameters of V-down ribs attached below the corrugated absorbing plate of SAH on the η_{t-th} has been examined. The impacts of key roughness parameters, including relative pitch p/e (6−12), relative height e/D (0.019−0.043), angle of attack α (30° −75°), and Re (1000−20000), are examined under real weather conditions. The SAH η_{t-th} roughened by V-down ribs is predicted using an in-house developed conjugate heat transfer numerical model. It has been shown that the maximum SAH η_{t-th} is 78.8%, predicted under steady-state conditions of Re = 20000, solar irradiance G =1000 W/m², p/e = 8, e/D = 0.043, and α =60. That is 15.7% more efficient than that of the default smooth surface. Under real weather condition, the η_{t-th} of the roughened SAH with single and double glass covers are 17.7% and 20.1%, respectively, higher than those of smooth SAH.

Keywords: Absorber plate; Roughened surface; Solar Air Heater; Thermal analysis; V-ribbed duct

Nomenclature

A_p	projection area	m²
b	half-height of v-corrugated duct	m
C_f	energy conversion factor	-
c_{p_a}	specific heat capacity of air	J/kg K
D	hydraulic diameter	m
e/D	relative roughness height	-
f	friction factor	-
h_c	convective heat transfer coefficient	W/m² K
h_r	radiative heat transfer coefficient	W/m² K
h_w	convective heat transfer coefficient	W/m² K
G	Solar irradiance	W/m²
L_1	length of the collector	m
L_2	width of the collector	m
$\dot{m}$	mass flowrate	kg/s
Nu	Nusselt number	-

Preprints (www.preprints.org) | NOT PEER-REVIEWED | Posted: 30 May 2022 doi:10.20944/preprints202205.0389.v1

p/e	relative roughness pitch	-
P_m	power consumption	W
Q_u	useful energy	W
Re	Reynolds number	-
T	temperature	K
t_i	thickness of insulation	m
U_b	coefficient of bottom heat loss	W/m^2 K
U_t	coefficient of top heat loss	W/m^2 K
V_w	wind speed	m/s
W	width of absorber plate	m
Greek letters		
α	angle of attack	°
α_p	absorptivity of absorbing plate	-
β	tilted angle of collector	°
σ	Stefan–Boltzmann constant	W/m K^4
ρ_a	density of air	kg/m^3
λ	thermal conductivity	W/m K
μ_a	viscosity of air	Pa s
$\eta_{t\text{-}th}$	total-thermal efficiency	%
η_{th}	thermal efficiency	%
ε	emittance	-
τ_c	transmissivity of the glass cover	-
ΔP	pressure drop	Pa
Subscripts		
a	air	
ai	inlet air	
am	ambient air	
ao	outlet air	
b	backplate	
b-a	backplate to air	
i	insulation	
p	absorber plate	
p-a	absorber plate to air	
p-b	absorber plate to bottom plate	

 doi:10.20944/preprints202205.0389.v1

1. Introduction

The world is concerned about the global environmental degradation and growing energy consumption, which acquire prominence in the near future. It is critical for a society to shift toward accessible renewable energy resources and maintain the balance between sustainability and economic benefits [1]. The utilization of renewable energy sources for the daily energy needs is rapidly growing. Solar energy is an essential source of renewable energy that may be used in a variety of ways, including direct/indirect heating, and photovoltaic power generation [2,3]. The solar air heater (SAH) collector is essential for solar energy conservation, which has several uses in the sectors of heating and drying [4]. SAH heats up the surrounding air, which can subsequently be utilized for a variety of purposes, including heating, cooling, and drying. SAHs are relatively cheap to buy and maintain. However, it has a low thermal efficiency because of low thermo-physical characteristics of the air in the laminar sub-layer region over the heated absorber plate [5]. Artificial roughness of various patterns on the absorber plate can be used to alleviate the sub-layer disadvantage and improve the system effectiveness [6–8].

In recent years, creating artificial roughness on the SAH absorber plate has been a popular study topic for many researchers (e.g., [9,10]). A study by Prasad et al. [11] presents a SAH roughened by small diameter wires, which has shown a remarkable enhancement in the SAH performance. The wire generates turbulence over the heated surface, breaking the laminar sub-layer and increasing the convective heat transfer coefficient. The impacts of W-shaped ribs characteristics in a duct flow on the performance of SAH are investigated in [12]. The results reveal the maximum increases in Nusselt number (Nu) (2.36 times) and in friction factor (f) (2.01 times).

Hans et al. [13] facilitated multiple V-ribs to roughen the absorber plate of a SAH, which resulted in a higher convective heat transfer coefficient. In the latter study, it was shown that Nu increased by 6 times when compared to the smooth SAH, while f increased by 5 times. Also, Momin et al. [14] used V-rib with α = 60°, who found

Preprints (www.preprints.org) | NOT PEER-REVIEWED | Posted: 30 May 2022 doi:10.20944/preprints202205.0389.v1

that *Nu* increased by a factor of 1.14 compared with that of the inclined ribbed SAH. Therefore, The V-ribs SAHs had noticeable benefits over the inclined ribs ones under the same operation conditions. A numerical study of the SAH roughened by multiple V-ribs was conducted by Jin et al. [15], which improved the heat transfer considerably, and the thermal performance up to 2.35. Istanto et al. [16] made experimental investigation into the influence of α in the V-down ribs on the heat transfer coefficient and friction factor across SAH duct. They claimed that as compared to the smooth absorbing plate, the greatest augmentation of Nu and *f* were 2.34 and 2.45 times. The technique of gaps in V-rib was used by Karwa et al. [17] to induce turbulence at several spots along the flow direction across the SAH.

According to the abovementioned literature, the roughened SAH absorbing plate improves the system thermal efficiency. As such, there is a significant rise in pressure drop throughout the system, and consequently increased power consumption. In our analysis, the impacts of V-down ribs on SAH are investigated for a wide range of Re. The influence of the V-down rib SAH geometrical parameters, such as *p/e*, *e/D*, and α, on its thermal efficiency is numerically examined and validated, under real weather conditions. Also, the SAH η_{t-th} roughened by V-down ribs is predicted using an in-house developed conjugate heat transfer numerical model. The thorough literature has not been giving enough focus on this matter; hence, the work originality is noticeable in contribution to this field of study. In what follows, the analysis and models are detailed in Section 2. In Section 3, the results and illustrative date are presented. The results are summarised in Section 4.

2. The model

As explained in earlier section, the SAH with artificial roughness is expected to perform better than smooth surface SAH. This can be attributed to the artificial roughness, leading to enhanced heat transfer and hence heat

Preprints (www.preprints.org) | NOT PEER-REVIEWED | Posted: 30 May 2022 doi:10.20944/preprints202205.0389.v1

transfer coefficient. In addition, the presence of the roughness elements on the heated surface accounts for thinning the absorber plate viscous sub-layer. Also, the thermal efficiency of a corrugated SAH is better than that of a flat plate SAH [18]. In this work, both effects are included which are corrugated absorber plate and V-down ribs on the backside of the heated surface, as indicated in Fig. 1, is studied. The SAH with a 60° corrugation angle consists of a 4 mm glass cover, a 1 mm absorbing and bottom plates, a 50 mm back insulation. The air flows via an equilateral triangle channel created by the combination of the absorber and bottom plates. Two SAHs with equal components and dimensions are investigated, one with V-down ribs and one without. To derive the energy balance equation for each component of the SAH without distorting the basic physical condition, the following assumptions are used [19]:

- The SAH is modelled using a steady-state assumption.
- The heat transfer between the components of a SAH is one-dimensional.
- The SAH's side heat losses are neglected, and there is no air seepage from the collector.
- At sky temperature, thermal radiation occurs between the SAH and its surroundings.

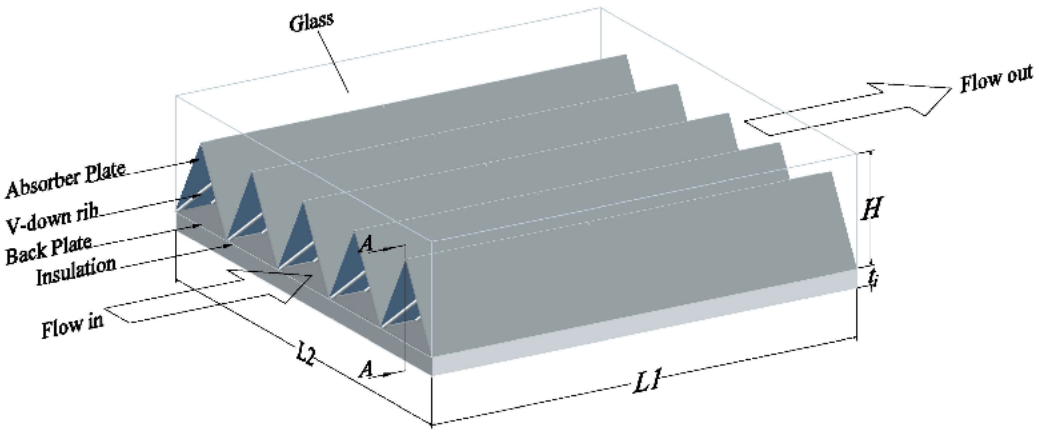

(a)

Preprints (www.preprints.org) | NOT PEER-REVIEWED | Posted: 30 May 2022 doi:10.20944/preprints202205.0389.v1

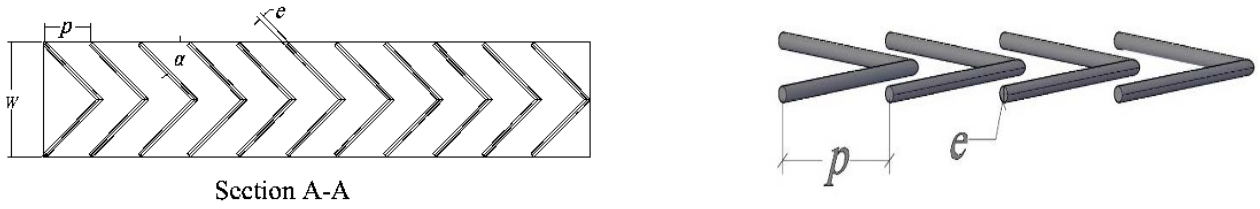

(b) (c)

Fig. 1. Schematic diagram of (a) SAH components (b) section A-A shows V-down ribs, and (c) zoomed-in view of V-down ribs.

2.1. Energy analysis

The SAH with roughed heated surface has the same thermal behaviour as that of traditional SAH as in both collectors. The absorber plate absorbs the solar irradiance and transfer the heat to the air. Thereby, the same approach that is used to determine insolation and heat losses for traditional SAH could be used for roughened SAH. A schematic diagram of the energy flow between SAH components is depicted in Fig. 2. Based on the energy flow diagram, the energy balance equations per unit area for the absorber plate, air, and backplate are expressed as:

$$\tau_c\,\alpha_p G = U_t(T_p - T_{am}) + h_{r,p-b}(T_p - T_b) + h_{c,p-a}(T_p - T_a), \quad (1)$$

$$\frac{2\dot{m}\,cp_a}{A_p}(T_a - T_{ai}) = h_{c,p-a}(T_p - T_a) + h_{c,b-a}(T_b - T_a), \quad (2)$$

$$h_{r,p-b}(T_p - T_b) = h_{c,b-a}(T_b - T_a) + U_b(T_b - T_{am}). \quad (3)$$

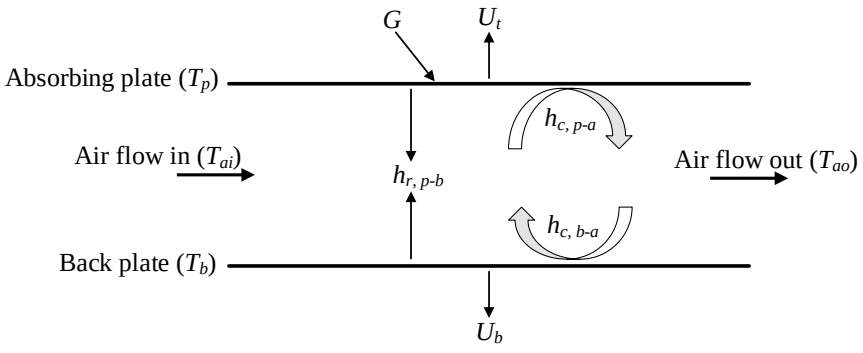

Fig. 2. Energy flow diagram between SAH elements.

A large number of loss coefficient is related to flat plate solar collectors. The following correlation (suggested by Malhotra et al. [20]) was used to calculate the top loss coefficient (U_t):

Preprints (www.preprints.org) | NOT PEER-REVIEWED | Posted: 30 May 2022 doi:10.20944/preprints202205.0389.v1

$$U_t = \left[\frac{M}{\left(\frac{C}{T_p}\right)\left(\frac{T_p - T_{am}}{M+f}\right)^{0.33}} + \frac{1}{h_w}\right]^{-1} + \left[\frac{\sigma\left(T_p^2 + T_{am}^2\right)\left(T_p + T_{am}\right)}{\frac{1}{\epsilon_p + 0.05M\left(1-\epsilon_p\right)} + \frac{2M+f_m-1}{\epsilon_c} - M}\right], \quad (4a)$$

where L is the spacing between the cover and absorber plate, M is the number of glasses covers, f_m and C are calculated as:

$$f_m = \left(\frac{9}{h_w} - \frac{30}{h_w^2}\right)\left(\frac{T_{am}}{316.9}\right)(1 + 0.091M), \quad (4b)$$

$$C = 204.429\ (\cos\beta\ )^{0.252}\ L^{-0.24}. \quad (4c)$$

The convection heat transfer coefficient owing to the wind (h_w) is calculated by [19]:

$$h_w = 5.7 + 3.8\ V_w. \quad (5)$$

Back loss coefficient (U_b) is determined by using thermal conductivity (λ_i) and thickness (t_i) of insulation as [19]:

$$U_b = \frac{\lambda_i}{t_i}. \quad (6)$$

The convective heat transfer coefficient of airflow over the absorber plate is equal to that between air and back-plate as suggested by Hedayatizadeh [21], and calculated as:

$$h_{c,p-a} = h_{c,b-a} = \frac{3\lambda_a\ \mathrm{Nu}}{4b}, \quad (7)$$

where b is the half-height of the flow channel and λ_a is the thermal conductivity of air.

For a smooth triangular conduit, Nu is proportional to the Reynolds number (Re). As a result, before deciding which Nu equation to utilize, Re must be determined first [22].

$$\mathrm{Re} = \frac{4\ \rho_a\ V_{in}\ b}{3\mu_a}, \quad (8)$$

where V_{in} is the inlet air velocity.

Hollands and Shewen [22] recommended the following relation for Nu inside triangular conduit of SAH, which can be stated as:

$$\mathrm{Nu} = \mathrm{Nu}_1 + \gamma_1 \frac{b}{L_1} n, \quad (9)$$

Preprints (www.preprints.org) | NOT PEER-REVIEWED | Posted: 30 May 2022 doi:10.20944/preprints202205.0389.v1

where n is the number of collectors connected in series, and Nu_1 and γ_1 are functions of Re. For various flow conditions, Hollands and Shewen [22] suggested the following relationships for Nu_1 and γ_1:

$$\mathrm{Nu}_1 = 2.821 \text{ and } \gamma_1 = 0.126\mathrm{Re} \quad \text{for } \mathrm{Re} < 2800, \tag{10a}$$

$$\mathrm{Nu}_1 = 1.9 \times 10^{-6}\mathrm{Re} \text{ and } \gamma_1 = 225 \quad \text{for } 2800 \leq \mathrm{Re} \leq 10^4, \tag{10b}$$

$$\mathrm{Nu}_1 = 0.0302\mathrm{Re}^{0.74} \text{ and } \gamma_1 = 0.242\mathrm{Re}^{0.74} \quad \text{for } 10^4 < \mathrm{Re} < 10^5. \tag{10c}$$

For a SAH having V-down ribs on the absorbing plate, the *Nu* is determined from an empirical equation which was correlated by Hans et al. [13] as follows:

$$\mathrm{Nu}_r = 3.35 \times 10^{-5}\mathrm{Re}^{0.92}\left(\frac{e}{D}\right)^{0.77}\left(\frac{W}{w}\right)^{0.43}\left(\frac{\alpha}{90}\right)^{-0.49}\exp\left[-0.61\left(ln\left(\frac{\alpha}{90}\right)\right)^2\right] \times \left(\frac{p}{e}\right)^{8.54} \times \exp\left[-2.0407\left(\ln\left(\frac{p}{e}\right)\right)^2\right] \times \exp\left[-0.1177\left(ln\left(\frac{W}{w}\right)\right)^2\right] \tag{11}$$

The thermal radiation coefficient between the absorber and backplates can be calculated as [19]:

$$h_{r,p-b} = \frac{\sigma\left(T_p^2+T_b^2\right)\left(T_p+T_b\right)}{\frac{1}{\epsilon_p}+\frac{1}{\epsilon_b}-1}. \tag{12}$$

The following empirical correlations were suggested by Gao et al. [23] to determine the density, dynamic viscosity and thermal conductivity of air, respectively:

$$\rho_a = 3.9147 - 0.016082\,T_f + 2.9013 \times 10^{-5}\,T_f^2 - 1.9407 \times 10^{-8}\,T_f^3, \tag{13}$$

$$\mu_a = \left(1.6157 + 0.06523\,T_f - 3.0297 \times 10^{-5}T_f^2\right) \times 10^{-6}, \tag{14}$$

$$\lambda_a = \left(0.0015215 + 0.097459\,T_f - 3.3322 \times 10^{-5}\,T_f^2\right) \times 10^{-3}, \tag{15}$$

where T_f is the average air temperature across the SAH in Kelvin, which is computed as $T_f = (T_{ao} + T_{ai})/2$. The specific heat at constant pressure of air (c_{pa}) is assumed equal to 1006 J/kg K.

2.2. Performance analysis

The thermal efficiency (η_{th}) of a SAH based on the 1st law of thermodynamics can be defined as the ratio of the useful energy gain (Q_u) to the solar irradiance over a time period [19], as:

Preprints (www.preprints.org) | NOT PEER-REVIEWED | Posted: 30 May 2022 doi:10.20944/preprints202205.0389.v1

$$\eta_{th} = \frac{Q_u}{GA_p} = \frac{\dot{m}\, cp_a(T_{ao}-T_{ai})}{GA_p}. \quad (16)$$

Total-thermal efficiency (η_{t-th}) is defined as the effect of useful heat gain minus power consumption by the fan that drives air through the SAH channels over a time period to the solar irradiance over the same period. It's crucial for determining whether an increase in pressure drop improves thermal efficiency. As a result, $\eta_{t\text{-}th}$ indicates the SAH's actual economic performance, which can be calculated as [24]:

$$\eta_{t-th} = \frac{Q_u - \frac{P_m}{C_f}}{GA_p}, \quad (17)$$

It is necessary to refer that the energy losses associated with the generation of the power consumed by the fan. Following [10,25,26] , these losses are assumed as follows: the fan efficiency η_f= 0.65, the efficiency of the electric motor η_m = 0.88, the efficiency of electrical transmission from the power plant η_{tr} = 0.92 and the thermal conversion efficiency of the power plant $\eta_{thc} = 0.35$. These coefficients can be shortened in a one named conversion correction factor (C_f), which has a value of 0.18.

where P_m is the mechanical power consumed by the blower to force the air throughout the SAH, which can be calculated as [27]:

$$P_m = \frac{\dot{m}\,\Delta P}{\rho_a}. \quad (18)$$

The pressure drop across the SAH (ΔP) is determined as [28]:

$$\Delta P = \frac{4\rho_a L V_{in}^2 f}{2D}, \quad (19)$$

f is the friction factor, calculated using the Hedayatizadeh *et al.* [21] Relations for smooth SAH as:

$$f = f_1 + \phi \frac{b}{L_1} n, \quad (20)$$

f_1 and ϕ are functions of the *Re* number, determined as:

$$f_1 = 13.33\mathrm{Re}^{-1} \text{ and } \phi = 0.65 \qquad \text{for } \mathrm{Re} < 2800, \quad (21a)$$

$$f_1 = 3.2 \times 10^{-4}\mathrm{Re}^{0.34} \text{ and } \phi = 2.94\mathrm{Re}^{-0.19} \text{ for } 2800 \le \mathrm{Re} \le 10^4, \quad (21b)$$

Preprints (www.preprints.org) | NOT PEER-REVIEWED | Posted: 30 May 2022 doi:10.20944/preprints202205.0389.v1

$$f_1 = 0.0733\mathrm{Re}^{-0.25} \text{ and } \phi = 0.51 \qquad \text{for } 10^4 \le \mathrm{Re} \le 10^5. \tag{21c}$$

For SAH having V-down ribs on the absorbing plate, the following empirical correlation is used to estimate f [13]:

$$f_r = 0.000447\mathrm{Re}^{-0.3188}\left(\frac{e}{D}\right)^{0.73}\left(\frac{W}{w}\right)^{0.22}\left(\frac{\alpha}{90}\right)^{-0.39}\exp\left[-0.52\left(ln\left(\frac{\alpha}{90}\right)\right)^2\right]\left(\frac{p}{e}\right)^{8.9}\exp\left[-2.133\left(\ln\left(\frac{p}{e}\right)\right)^2\right]. \tag{22}$$

In order to validate between current numerical and other experimental results reported by other researchers, the root-mean-square error was used here. The degree of concordance between the mathematical (x_i) and experimental (y_i) findings of the smooth SAH was quantified using statistical analysis. The root-mean-square error (RMSE) is determined as [4]:

$$\mathrm{RMSE} = 100\sqrt{\frac{\sum_1^N\left(\frac{x_i-y_i}{x_i}\right)^2}{N}}. \tag{23}$$

2.3. Numerical algorithm

Based on the energy flow equations 1 – 3, there have not been sufficient analytical solutions to the temperatures of the SAH components, like: T_p, T_b, and T_a. Also, the efficiencies and most coefficients of the heat transfer are functions of these temperatures. Therefore, temperatures, efficiencies, and heat transfer coefficients are determined numerically by iterations. All relevant computations are programmed using an in-house developed MATLAB code (version R2019b). The solution technique begins by calculating the heat transfer coefficients based on guessed temperatures, which are subsequently used to predict new temperatures. The run loop is iterative until reaching *a priori* value of 0.001%, obtained from the absolute difference between the old and updated temperatures ($|T_{\text{new}} - T_{\text{old}}|$). The process will be continued until the absolute difference became equal or less than 0.001%. The values of fixed and variable input parameters used in the MATLAB code are shown in Table 1.

Table 1. Parameters used in our numerical solution.

Preprints (www.preprints.org) | NOT PEER-REVIEWED | Posted: 30 May 2022 doi:10.20944/preprints202205.0389.v1

Parameter	Value
A_p	1 m^2
W	2 m
L_1	1 m
N	5
t_i	5 cm
λ_i	0.079 W/m.°C
L_2	1 m
ε_p	0.95
ε_b	0.95
α_p	0.96
ε_c	0.9
τ_c	0.88
Re	1000 – 20,000
G	1000 W
T_{am}	25 °C
T_{ai}	28 °C
V_w	2.5 m/s
C_f	0.18
e/D	0.019 – 0.043
p/e	6 – 12
W/w	10
α	30°– 75°

2.4 Validation of the model

A comparison of the current results with the experimental data reported by Kabeel et al. [25] is used to verify the current model for smooth SAH as shown in Fig. 3. The maximum, minimum, and average percentage errors were 8.91%, 1.76%, and 6.26%, respectively, all of which are acceptable. The RMSE value for exit air temperature is 6.49%. The precision in measuring solar irradiance, ambient temperature, and wind speed, are all elements that contribute to such a notable difference between numerical and experimental results. Also, the accuracy with which optical characteristics were estimated, as well as the assumptions employed to build the mathematical model. Subsequently, it is clear that the present work results are in good agreement with the published studies

Preprints (www.preprints.org) | NOT PEER-REVIEWED | Posted: 30 May 2022 doi:10.20944/preprints202205.0389.v1

and the present model can be applied for further investigations. The variation of total-thermal performance parameter (TTPP) for rectangle SAH roughened by V-down rib with Re for different attack angles reported by Istanto et al. [16] was compared with present work as depicted in Fig. 4. The triangular channels utilized in this study had a greater TTPP than the rectangular channels used in the previous study, as seen in this figure. In addition, the trend for TTTP is the same in both graphs.

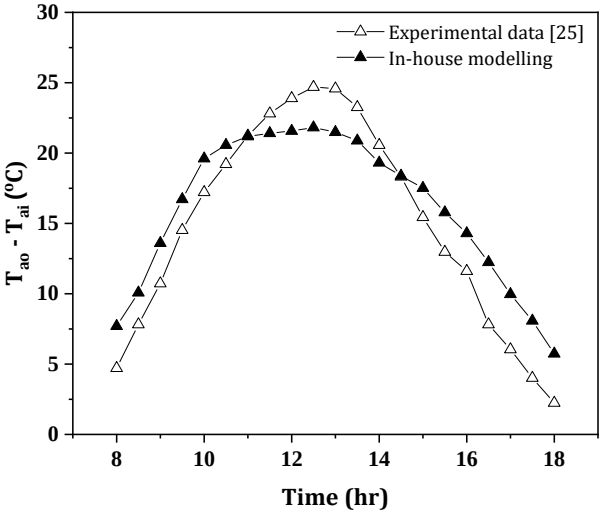

Fig. 3. Temperature difference across a smooth SAH ($T_{ao} - T_{ai}$) versus daytime hours using our in-house model predictions and experimental data inferred from [25].

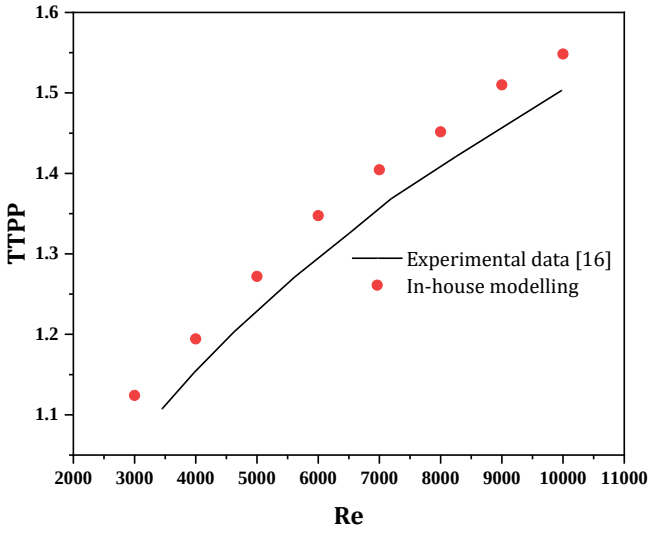

Fig. 4. TTPP versus Re based on our in-house predictions and experimental data inferred from [16].

Preprints (www.preprints.org) | NOT PEER-REVIEWED | Posted: 30 May 2022 doi:10.20944/preprints202205.0389.v1

3. Results

The useful energy, η_{th}, and $\eta_{t\text{-}th}$ of SAH roughened by V-down ribs, calculated based on the numerical solution for numerous flow and roughness characteristics, were discussed below. To examine the improvement in useful energy, η_{th}, and $\eta_{t\text{-}th}$ due to artificial roughness parameters, the findings were compared to those obtained in the case of smooth ducts operated under the same conditions.

The effect of Re on the useful energy with various values of p/e and fixed values of $\alpha = 55°$, $e/D = 0.031$, and $W/w = 10$ is depicted in Fig. 5a. Clearly, useful energy rapidly increases when Re increases. It means that as Re rises, the convective heat transfer coefficient rises as well. This might be due to flow slowing down, which creates an unfavourable pressure gradient, which increases instability, eddy formation, and flow separation at the protruded surface. As a result, a significant energy loss from the heated surface has been transferred to the working fluid. Fig. 5a shows that the maximum heat gain for a SAH roughened by V-down ribs is 778.9 W, compared to 655.2 W for a smooth SAH and that the increase in heat gain becomes stable at increasing Re levels. As a result, raising the Re over 20000 has no advantage to the thermal system; it merely adds more pumping power. It is observed from Fig. 5b that useful gain increases at first, then drops as p/e grows. At smaller values of p/e ($p/e < 8$), therefore decreasing the convective heat transfer coefficient. If the value of p/e is increased beyond a certain point ($p/e > 8$), however, it may not be able to break the laminar sub-layer, preventing the development of eddies and resulting in reduced convective heat transfer coefficient.

Preprints (www.preprints.org) | NOT PEER-REVIEWED | Posted: 30 May 2022 doi:10.20944/preprints202205.0389.v1

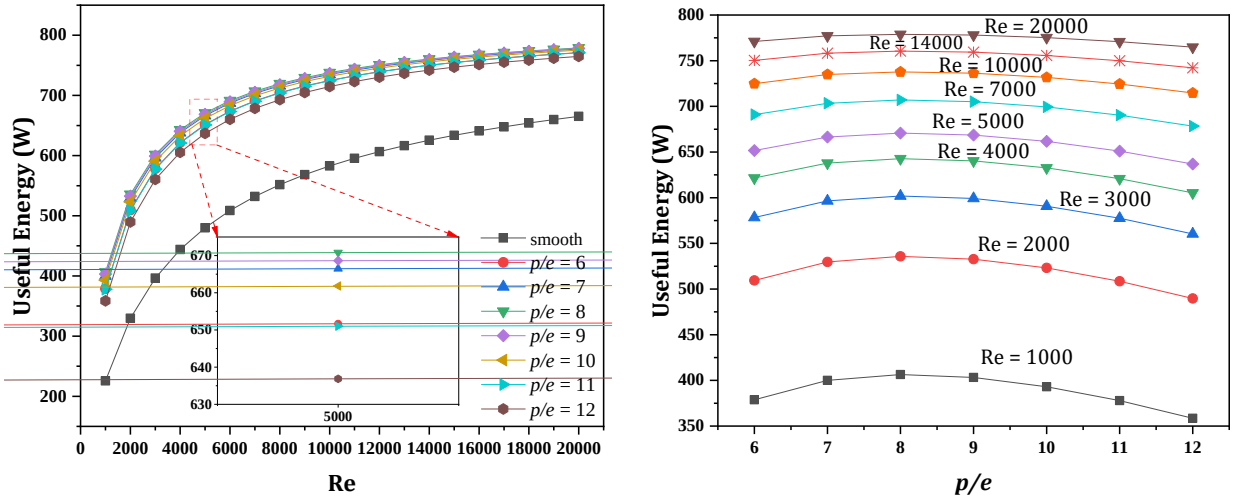

(a) (b)

Fig. 5. Useful energy versus (a) Re at various pitch ratios p/e (in the range 6 – 12) and (b) pitch ratios p/e at various Re (1000 – 20000).

In Fig. 6a, the influence of the V-down rib pitch ratio on the SAH's thermal efficiency is presented at fixed values of $\alpha = 55°$, $e/D = 0.031$, and $W/w = 10$ for a wide-ranging of Re. As the Re increases, the thermal efficiency increases fast as the heat gain rises. In addition, at high Re values, the gain in thermal efficiency becomes minimal in all cases (with and without ribs). It can be observed that the highest thermal efficiency for roughness SAH is 77.9% against 66.5% for smooth SAH. Essentially, in all thermal applications, including SAHs, maximum thermal efficiency, and minimal pressure drop are required. Therefore, the variation in specific parameters like useful gain and thermal efficiency does not clear the picture in terms of SAH thermal performance. As a result, hydro-thermal efficiency was investigated, which combines improved thermal efficiency with increased pressure drop. In Fig. 6b, the total-thermal efficiencies of SAH with and without V-down ribs are shown for a range of Re. In comparison to smooth SAH, the total-thermal efficiency is noticeably increased for all rib pitch ratios. According to the foregoing findings, the best total-thermal efficiency is achieved at $p/e = 8$ and $\mathrm{Re} = 20000$.

Preprints (www.preprints.org) | NOT PEER-REVIEWED | Posted: 30 May 2022 doi:10.20944/preprints202205.0389.v1

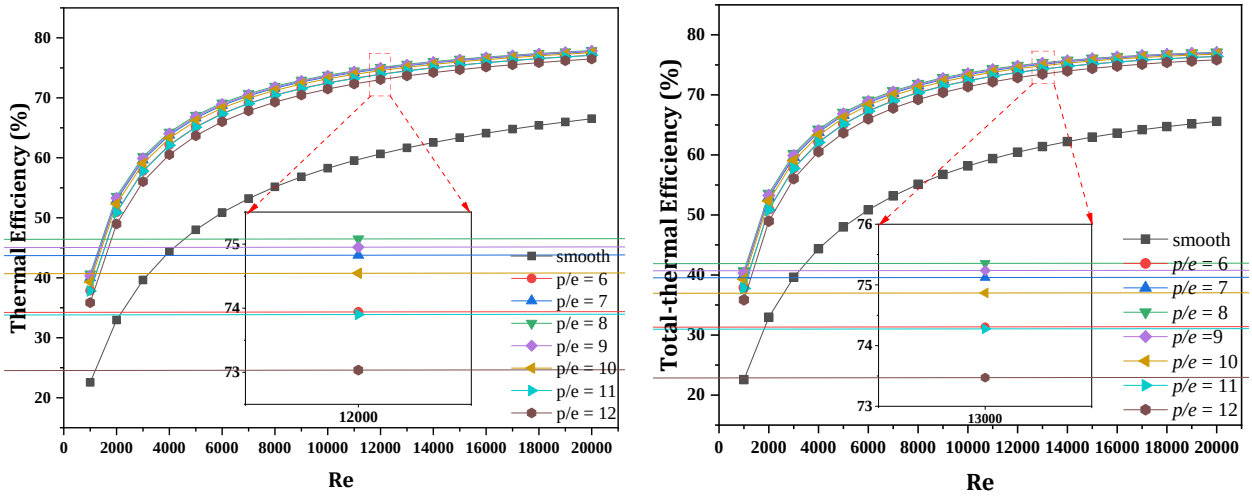

(a) (b)

Fig. 6. Thermal (a) and total-thermal (b) efficiencies versus Re for smooth and V-down rib roughened surfaces at various pitch ratios p/e (in the range 6 – 12).

The useful energy is investigated as a function of Re with various values of e/D and given values of $\alpha = 55°$, $p/e = 8$, and $W/w = 10$ (see Fig. 7). As one can see from Fig. 7, facilitating smaller ribs results in a significant increase in useful energy. When the rib height ratio rises, the augmentation becomes more noticeable. Due to intense turbulence induced in the main flow channel, which might promote mixing between the cold fluid and the heating surface, the increase in useful energy is noticeable at high values of Re. The useful energy can be increased up to 1.18 times that of a smooth SAH. On the other hand, when the rib height ratio is increased, the cross-sectional area of the flow channel is reduced, resulting in a larger pressure drop.

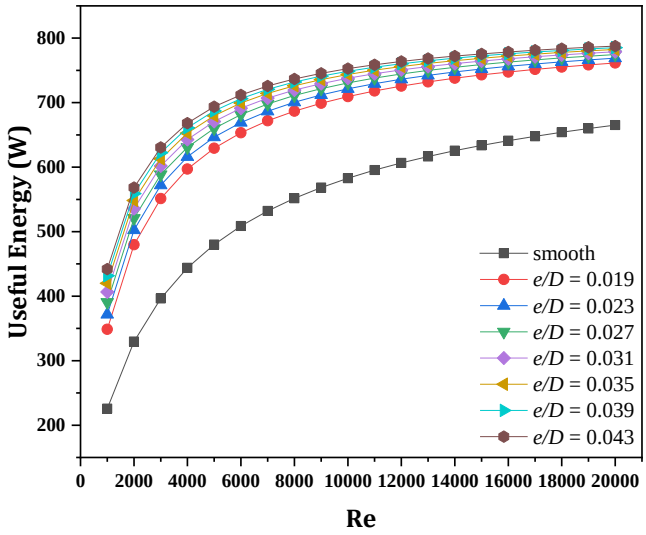

Preprints (www.preprints.org) | NOT PEER-REVIEWED | Posted: 30 May 2022 doi:10.20944/preprints202205.0389.v1

Fig. 7. Useful energy (W) versus Re for smooth and roughened surfaces at various relative roughness heights e/D (in the range 0.043 – 0.019).

The influence of relative roughness height on thermal efficiency over a wide range of Re is presented in Fig. 8. It can be concluded from this figure that a considerable gain in thermal efficiency is found when the V-down ribs are utilized at the lowest value of the Re, and this improvement enhances with increasing relative roughness height. For a specific value of e/D, this improvement is observed to be beneficial at lower Re and diminishes with rising Re until it reaches 20000, at which point it remains unchanged. In addition, useful energy increases with an increment in Re, as seen in Fig. 8a. As mentioned in the preceding section, this pattern is owing to the substantial breakdown of the laminar sub-layer at a high value of Re. It can be reported that the maximum increment in thermal efficiency is 16% which is obtained at Re = 20000, and e/D = 0.043. In Fig. 8b, total-thermal efficiency is shown against Re for all levels of relative roughness height. Greater total-thermal efficiency is associated with higher relative roughness height and/or higher Re. The total-thermal efficiency of a SAH with V-down rib at e/D = 0.043 is 77.8%, compared to 65.6 % for a smooth SAH at Re = 20000. The best total-thermal efficiency is found at Re = 20000 and e/D = 0.043, based on the above findings.

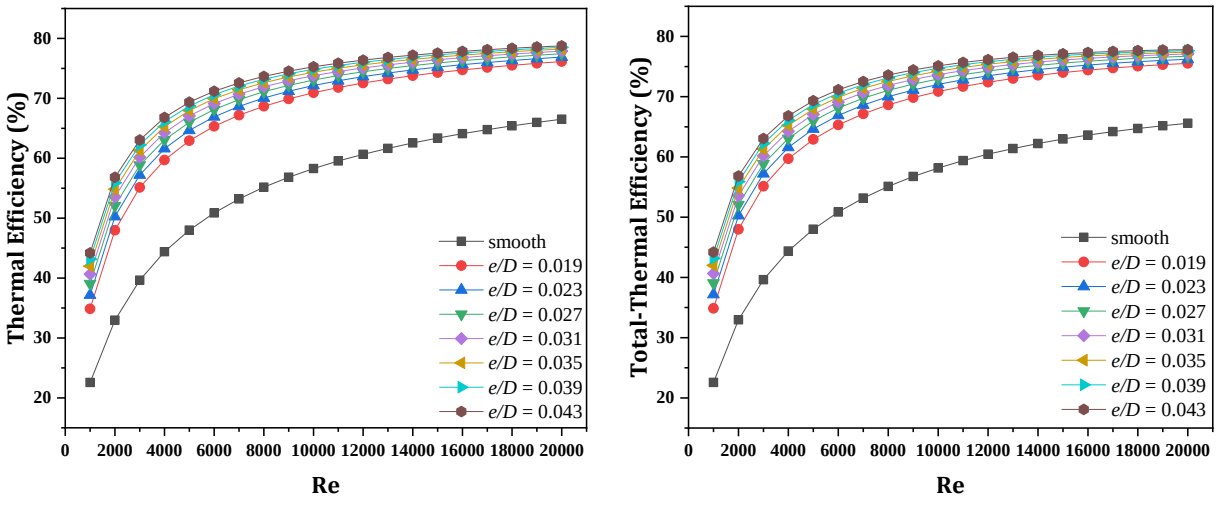

(a) (b)

Fig. 8. Thermal (a) and total-thermal (b) efficiencies versus Re at smooth and roughened surfaces various relative roughness heights (in the range 0.043 – 0.19).

Preprints (www.preprints.org) | NOT PEER-REVIEWED | Posted: 30 May 2022 doi:10.20944/preprints202205.0389.v1

The variations in useful energy as a function of angle of attack for various values of Re and given values of $e/D = 0.043$, $p/e = 8$, and $W/w = 10$ have been shown in Fig. 9a. For any given Re, useful energy rises as the angle of attack rises, peaking at 60°. Useful energy decreases as the angle of attack is increased above 60°. It can be observed that there is a value of angle of attack for which useful energy reaches its maximum. The presence of V-down ribs may cause flow separation, with the movement of ensuing vortices combining to produce an optimal angle of attack. Useful energy increases fast with an increase in the angle of attack, as seen in Fig. 9b, and then progressively declines with a higher angle of attack values. The effect of angle of attack on useful energy follows the same pattern as p/e.

For a wide range of Re, Fig. 10a shows the effect of the angle of attack on the thermal efficiency for fixed values of $p/e = 8$, $e/D = 0.043$, and $W/w = 10$. As Re rises, so does the thermal efficiency as the heat gain increases. Furthermore, the improvement in thermal efficiency is limited at high Re values in all cases. It can be reported that the maximum thermal efficiency is 78.8% occurred at $\alpha = 60°$ and Re = 20000. Fig. 10b illustrates how the total-thermal efficiency varies with the angle of attack over a range of Re. Total-thermal efficiency is considerably higher for all angles of attack as compared to smooth SAH.

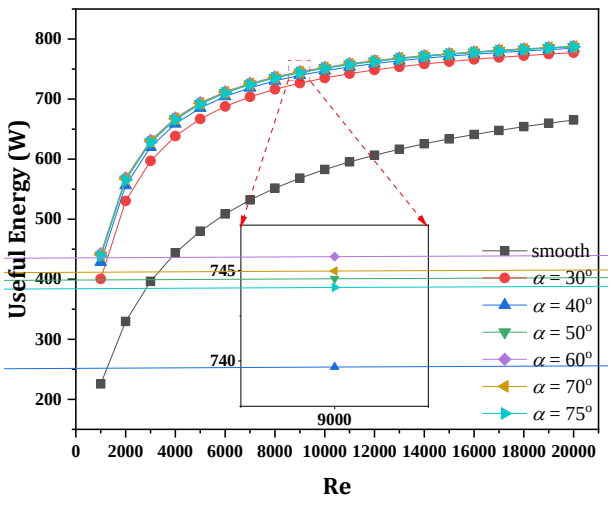

(a)

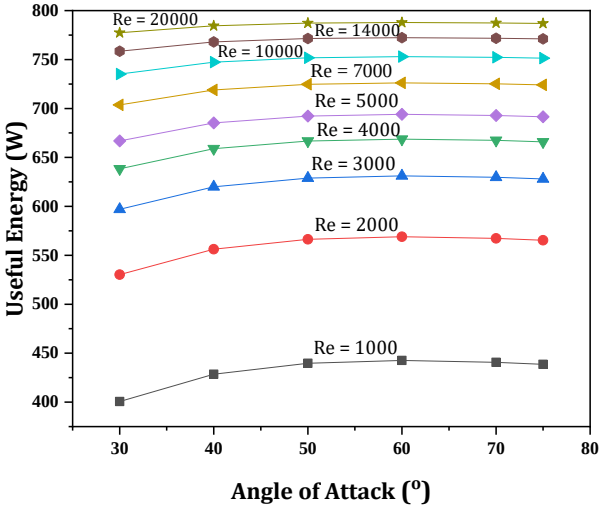

(b)

Preprints (www.preprints.org) | NOT PEER-REVIEWED | Posted: 30 May 2022 doi:10.20944/preprints202205.0389.v1

Fig. 9. Useful energy versus (a) Re at various angles of attack (in the range 30° – 75°) and (b) angles of attack at various Re (in the range 1000 – 14000).

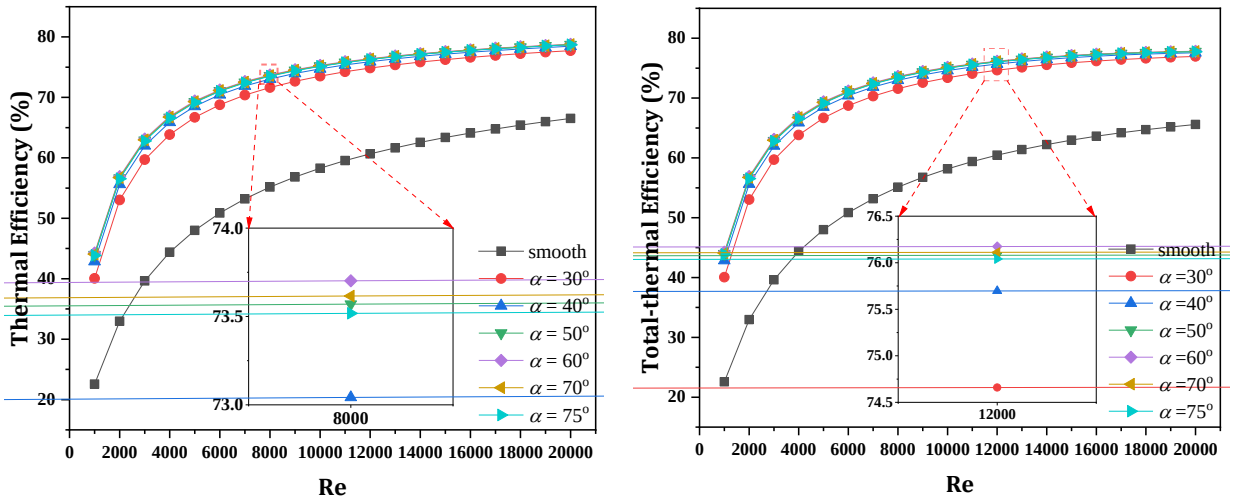

(a) (b)

Fig. 10. Re at various angles of attack (in the range 30° – 75°) versus the (a) thermal efficiency and (b) total-thermal efficiency.

Based upon the above results, the optimal V-down rib parameters which gives maximum total-thermal efficiency are $p/e = 8$, $e/D = 0.043$, and $\alpha = 60°$ These parameters are examined theoretically of a SAH at Re = 20000, and real weather conditions of Baghdad, Iraq (33.3 $°N$, 44.4 $°E$). Table 2 shows the values of insolation, ambient temperature, and wind velocity for a typical sunny day in January, which was taken from a local weather station.

Table 2. Weather data of a typical sunny day in Baghdad city on 14th January 2021.

Time (hr)	8:00	9:00	10:00	11:00	12:00	13:00	14:00	15:00	16:00
G (W/m²)	282.1	598.4	821.2	964.3	1025.1	1001.2	849.6	707.2	436.3
T_{amb} (°C)	8.1	9.0	10.2	11.5	13.0	13.7	14.5	15.0	14.3
V_w (m/s)	2.8	4.2	5.8	6.1	6.4	6.7	6.7	6.4	6.1

The influence of the optimal V-down rib parameters on the useful energy of SAH as a function of daytime is presented in Fig. 11a. Clearly from the latter figure, the useful energy rises during the day, peaks at midday, and then falls in the afternoon. During the day, it fluctuates according to the insolation. It can be observed that the use of a double glass cover with rib roughness will give more enhancement in the useful heat gain. At noon, the maximum useful energy for smooth with a single cover, roughness with a single cover, and roughness with double covers is 660.8, 801.4, and 825.4 W, respectively. Fig. 11b shows the thermal efficiency of a SAH with and without

Preprints (www.preprints.org) | NOT PEER-REVIEWED | Posted: 30 May 2022 doi:10.20944/preprints202205.0389.v1

ribs inside its channels as a function of day hours for single and double covers. The thermal efficiency improves for two hours after sunrise for all patterns and then remains relatively constant for the rest of the day until one hour before sundown. The average thermal efficiency for a smooth SAH is 64.4% can be increased to 77.5% by using ribs with a single cover, furthermore, an improvement could be reached to 80.0% by using ribs and double covers. A similar pattern can be seen in Fig. 11c for total-thermal efficiency as well as thermal efficiency. The total-thermal efficiency of SAH having ribs with single and double covers is 17.7% and 20.1% higher, respectively than that of smooth SAH.

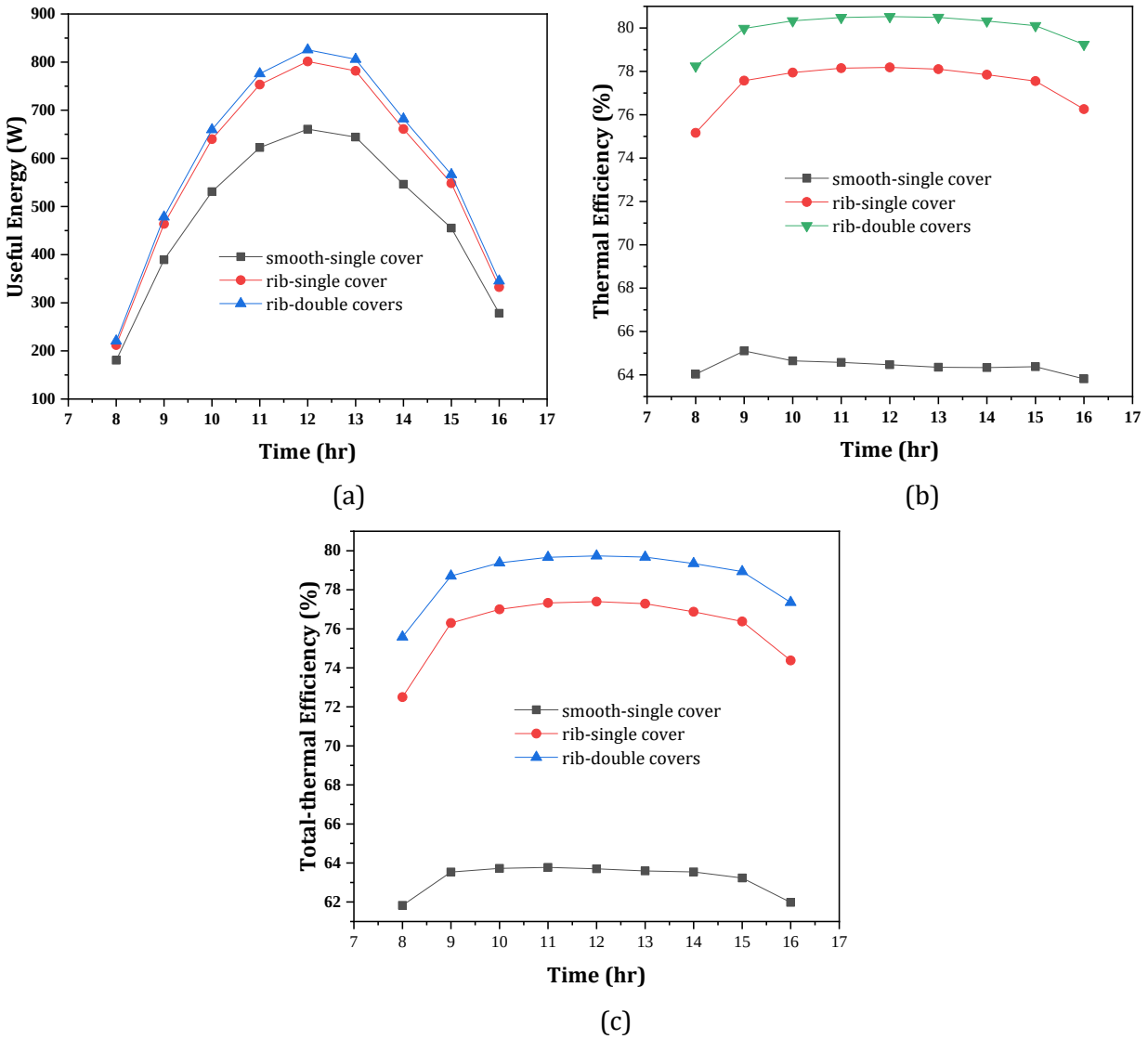

Fig. 11. Useful energy (a), thermal efficiency (b), and total-thermal efficiency (c) versus daytime for smooth, v-rib roughened with single cover, and v-rib roughened with double cover SAH surfaces at Re = 20000.

 doi:10.20944/preprints202205.0389.v1

4. Conclusions

This work presented a detailed examination into the operating characteristics of Solar Air Heaters (SAHs), with V-down rib roughness, on their absorber plates. The introduced in-house model, based on the solution to conjugate heat transfer equations and system performance characteristics, was aimed at determining the best roughness parameters for optimal system total-thermal efficiency. The primary findings of our study can be summarised as follows:

- The total-thermal efficiency was found to be optimum at p/e = 8, e/D = 0.043, and α =60°. The total-thermal efficiency of SAH with v-down ribs was 15.7 % higher than that of smooth SAH.
- The enhancement in useful energy of a roughened SAH was 1.18 times larger than that of a smooth SAH.
- The maximum thermal efficiency of a SAH roughened by V-down ribs is 78.8%, compared with 66.5% of that for a smooth SAH.
- Under actual weather conditions, the total-thermal efficiencies of SAH with V-down ribs are up to 17.7%, when using a single cover, and 20.1%, when using a double cover, higher than that of a smooth SAH.
- The present work results are in good agreement with the published studies with maximum percentage errors of 8.91%.

CRediT author statement

Mustafa Alaskari: Methodology, Software, Validation; **Arwa M. Kadhim:** Visualization, Investigation; **Ammar A. Farhan:** Conceptualisation, Writing- Original draft preparation, Supervision; **Moustafa Al-Damouk:** Writing – Review and Editing; **Mansour Al Qubeissi:** Writing- Reviewing and Editing, Data curation.

Preprints (www.preprints.org) | NOT PEER-REVIEWED | Posted: 30 May 2022 doi:10.20944/preprints202205.0389.v1

Appendix A. Solution algorithm

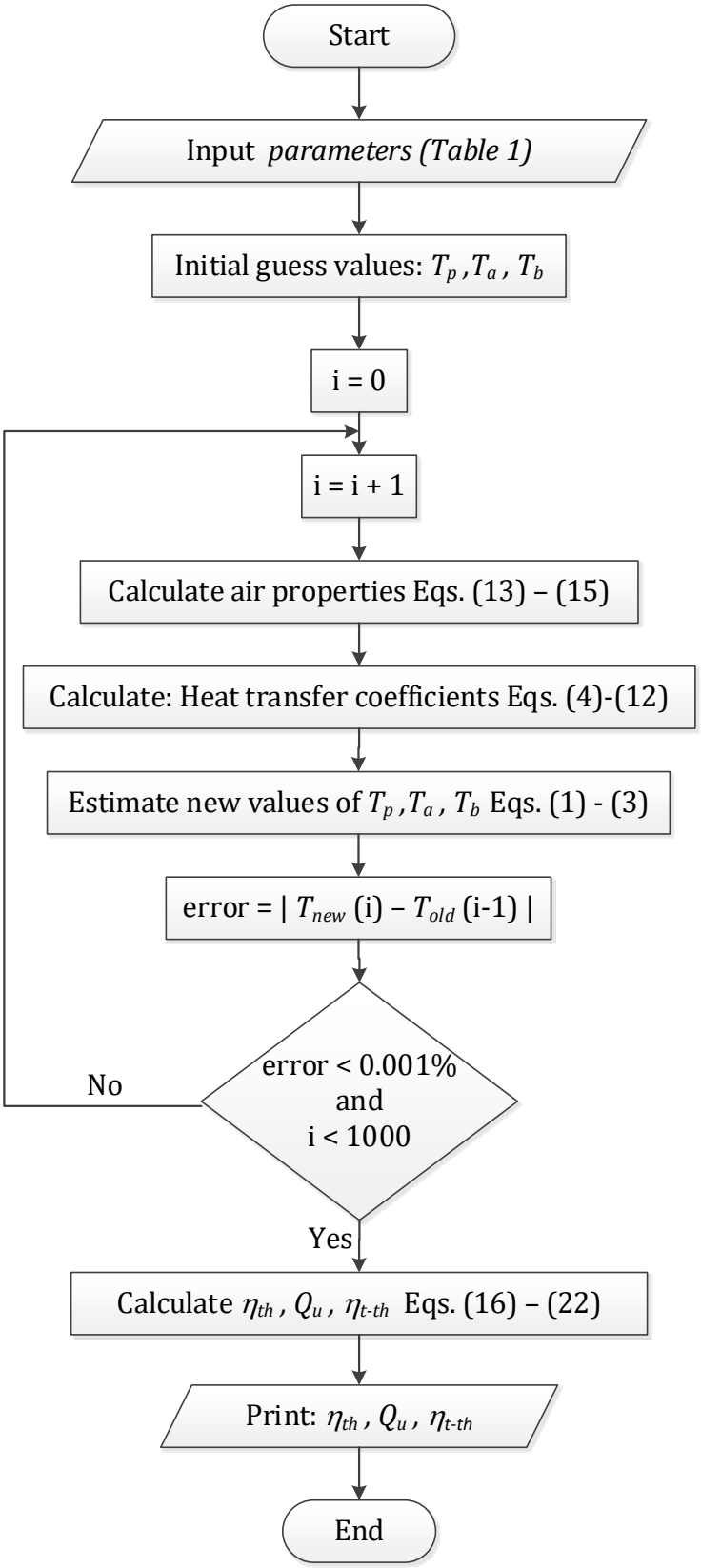

Fig. A1. Flowchart of the summarised logic algorithms of the in-house code.

References

[1] M. Al Qubeissi, A. El-kharouf, H.S. Soyhan, Renewable Energy - Resources, Challenges and Applications, 1st editio, IntechOpen, 2020. https://doi.org/10.5772/intechopen.81765.

[2] M. Al-Damook, K. Waleed Abid, A. Mumtaz, D. Dixon-Hardy, P.J. Heggs, M. Al Qubeissi, Photovoltaic module efficiency evaluation: The case of Iraq, Alexandria Eng. J. (2021). https://doi.org/10.1016/j.aej.2021.11.046.

[3] D.J. Hasan, A.A. Farhan, The Effect of Staggered porous fins on the performance of Photovoltaic panel in Baghdad, J. Eng. 26 (2020) 1–13. https://doi.org/10.31026/j.eng.2020.08.01.

[4] M. Al-Damook, Z.A.H. Obaid, M. Al Qubeissi, D. Dixon-Hardy, J. Cottom, P.J. Heggs, CFD modeling and performance evaluation of multipass solar air heaters, Numer. Heat Transf. Part A Appl. 76 (2019) 438–464. https://doi.org/10.1080/10407782.2019.1637228.

[5] M.K. Sahu, M.M. Matheswaran, P. Bishnoi, Experimental investigation of augmented thermal and performance characteristics of solar air heater ducts due to varied orientations of roughness geometry on the absorber plate, Arch. Thermodyn. 41 (2020) 147–182. https://doi.org/10.24425/ather.2020.134576.

[6] K. Nidhul, A.K. Yadav, S. Anish, S. Kumar, Critical review of ribbed solar air heater and performance evaluation of various V-rib configuration, Renew. Sustain. Energy Rev. 142 (2021) 110871. https://doi.org/10.1016/j.rser.2021.110871.

[7] V.P. Singh, S. Jain, J. Gupta, Analysis of the effect of perforation in multi-v rib artificial roughened single pass solar air heater: - Part A, Exp. Heat Transf. 00 (2021) 1–20. https://doi.org/10.1080/08916152.2021.1988761.

[8] A.A. Farhan, H.A. Sahi, Energy Analysis of Solar Collector With perforated Absorber Plate, J. Eng. 23 (2017) 89–102.

[9] V.S. Hans, R.P. Saini, J.S. Saini, Performance of artificially roughened solar air heaters—A review, Renew. Sustain. Energy Rev. 13 (2009) 1854–1869. https://doi.org/10.1016/j.rser.2009.01.030.

[10] M. Al-Damook, Z. Khatir, M. Al Qubeissi, D. Dixon-Hardy, P.J. Heggs, Energy efficient double-pass photovoltaic/thermal air systems using a computational fluid dynamics multi-objective optimisation framework, Appl. Therm. Eng. 194 (2021) 117010. https://doi.org/10.1016/j.applthermaleng.2021.117010.

[11] B.N. Prasad, A. Kumar, K.D.P. Singh, Optimization of thermo hydraulic performance in three sides artificially roughened solar air heaters, Sol. Energy. 111 (2015) 313–319. https://doi.org/10.1016/j.solener.2014.10.030.

[12] A. Lanjewar, J.L. Bhagoria, R.M. Sarviya, Heat transfer and friction in solar air heater duct with W-shaped rib roughness on absorber plate, Energy. 36 (2011) 4531–4541. https://doi.org/10.1016/j.energy.2011.03.054.

[13] V.S. Hans, R.P. Saini, J.S. Saini, Heat transfer and friction factor correlations for a solar air heater duct roughened artificially with multiple v-ribs, Sol. Energy. 84 (2010) 898–911. https://doi.org/10.1016/j.solener.2010.02.004.

[14] A.-M. Ebrahim Momin, J.. Saini, S.. Solanki, Heat transfer and friction in solar air heater duct with V-shaped rib roughness on absorber plate, Int. J. Heat Mass Transf. 45 (2002) 3383–3396. https://doi.org/10.1016/S0017-9310(02)00046-7.

[15] D. Jin, S. Quan, J. Zuo, S. Xu, Numerical investigation of heat transfer enhancement in a solar air heater roughened by multiple V-shaped ribs, Renew. Energy. 134 (2019) 78–88. https://doi.org/10.1016/j.renene.2018.11.016.

[16] T. Istanto, D. Danardono, I. Yaningsih, A.T. Wijayanta, Experimental study of heat transfer enhancement in solar air heater with different angle of attack of V-down continuous ribs, in: AIP Conf. Proc., 2016: p. 060002. https://doi.org/10.1063/1.4949309.

[17] R. Karwa, R.D. Bairwa, B.P. Jain, N. Karwa, Experimental Study of the Effects of Rib Angle and Discretization on Heat Transfer and Friction in an Asymmetrically Heated Rectangular Duct, J. Enhanc. Heat Transf. 12 (2005) 343–355. https://doi.org/10.1615/JEnhHeatTransf.v12.i4.40.

[18] A.A. Farhan, A. Issam M.Ali, H.E. Ahmed, Energetic and exergetic efficiency analysis of a v-corrugated solar air heater integrated with twisted tape inserts, Renew. Energy. 169 (2021) 1373–1385. https://doi.org/10.1016/j.renene.2021.01.109.

[19] J.A. Duffie, W.A. Beckman, N. Blair, Solar Engineering of Thermal Processes, Photovoltaics and Wind, fifth edit, JohnWiley& Sons, Inc., Hoboken,New Jersey, 2020.

[20] A. Malhotra, H.P. Garg, A. Palit, Heat loss calculation of flat plate solar collectors, J. Therm. Eng. 2 (1981) 59–62.

[21] M. Hedayatizadeh, Y. Ajabshirchi, F. Sarhaddi, S. Farahat, A. Safavinejad, H. Chaji, Analysis of exergy and parametric study of a v-corrugated solar air heater, Heat Mass Transf. 48 (2012) 1089–1101. https://doi.org/10.1007/s00231-011-0957-7.

[22] K.G.T. Hollands, E.C. Shewen, Optimization of flow passage geometry for air-heating, plate-type solar collectors, J. Sol. Energy Eng. Trans. ASME. 103 (1981) 323–330. https://doi.org/10.1115/1.3266260.

[23] W. Gao, W. Lin, T. Liu, C. Xia, Analytical and experimental studies on the thermal performance of cross-corrugated and flat-plate solar air heaters, Appl. Energy. 84 (2007) 425–441. https://doi.org/10.1016/j.apenergy.2006.02.005.

[24] S.Q. Hussien, A.A. Farhan, The Effect of Metal Foam Fins on the Thermo-hydraulic Performance of a Solar Air Heater, Int. J. Renew. Energy Res. 9 (2019) 840–847.

[25] A.E. Kabeel, A. Khalil, S.M. Shalaby, M.E. Zayed, Experimental investigation of thermal performance of flat and v-corrugated plate solar air heaters with and without PCM as thermal energy storage, Energy Convers. Manag. 113 (2016) 264–272. https://doi.org/10.1016/j.enconman.2016.01.068.

[26] D. N. Moriasi, J. G. Arnold, M. W. Van Liew, R. L. Bingner, R. D. Harmel, T. L. Veith, Model Evaluation Guidelines for Systematic Quantification of Accuracy in Watershed Simulations, Trans. ASABE. 50 (2007) 885–900. https://doi.org/10.13031/2013.23153.

[27] S.Y. Taha, A.A. Farhan, Performance augmentation of a solar air heater using herringbone metal foam fins : An experimental work, Int. J. Energy Res. (2020) 1–13. https://doi.org/10.1002/er.5927.

[28] R. Kumar, P. Chand, Performance prediction of extended surface absorber solar air collector with twisted tape inserts, Sol. Energy. 169 (2018) 40–48. https://doi.org/10.1016/j.solener.2018.04.021.